

# Horizon-T Experiment Calibrations – MIP Signal from Scintillator and Glass Detectors

D. Beznosko <sup>1b</sup>, T. Beremkulov <sup>b</sup>, A. Iakovlev <sup>b</sup>, A. Duspayev <sup>b</sup>, M. I. Vildanova <sup>a</sup>, T. Uakhitov <sup>b</sup>,  
M. Yessenov <sup>b</sup>, V.V. Zhukov <sup>a</sup>

## Abstract

Horizon-T, a modern Extensive Air Showers (EAS) detector system, is constructed at Tien Shan high-altitude Science Station of Lebedev Physical Institute of the Russian Academy of Sciences at approximately 3340 meters above the sea level in order to study in the energy range above  $10^{16}$  eV coming from a wide range of zenith angles ( $0^\circ - 85^\circ$ ).

The detector includes eight charged particle detection points and a Vavilov-Cherenkov radiation detector. Each charged particle detector response is calibrated using single MIP (minimally ionizing particle) signal. The details of this calibration are provided in this article. This note is valid for data before March 2017 and will not be updated following any detector calibration and configuration changes as a large upgrade has been implemented.

## 1. Detector System Brief Description

Tien Shan high-altitude Science Station, a part of Lebedev Physical Institute of the Russian Academy of Sciences, is located 32 km from the city of Almaty at the altitude of  $\sim 3340$  meters above the sea level. “Horizon-T” (HT) detector system [1] [2] is constructed to study space-time distribution of the charged particles in EAS disk and Vavilov-Cherenkov radiation from it with parent particle of energies higher than  $10^{16}$  eV coming from a range of zenith angles ( $0^\circ-85^\circ$ ). The novel method of using time information from pulse shape in each detector allows for the analysis of EAS with core falling outside of the detector system bounds.

HT consists of eight charged particles detection points and a detection of the Vavilov-Cherenkov radiation (VCD). The relative coordinates of every station and distances from station 1 are presented in Table 1. The aerial view of HT with detection points marked is in Figure 1.

All detection points and VCD connect to Data Acquisition system (DAQ) via cables. The cable calibration procedure and results are given in [3]. There are plans to upgrade the detector system to cable-less [4]. In order to study the spatial distribution of charged particles in EAS disk, an accurate calibration to a single particle response is required.

## 2. Near and Far Periphery Detectors

The near periphery combines the detection points 1, 4, 5, 6 and 7. Each of these detection points has one scintillator detector (SD) and one glass detector (GD). Both types have a pyramid shape with height equal to the side. Each SD is based on polystyrene square-shaped cast [5]

---

<sup>1</sup> [dmitriy.beznosko@nu.edu.kz](mailto:dmitriy.beznosko@nu.edu.kz) (also [dima@dozory.us](mailto:dima@dozory.us))

<sup>a</sup> P. N. Lebedev Physical Institute of the Russian Academy of Sciences, Moscow, Russia

<sup>b</sup> Physics Department, Nazarbayev University, Astana, Kazakhstan

scintillator [6] that has 1 m<sup>2</sup> area and is 5 cm thick. Each GD is based on 50 cm x 50 cm x 3 cm optical glass that is painted white with TiO<sub>2</sub> at the bottom side [7]. Both have the PMT above the scintillator/glass center. All near detectors use Hamamatsu [8] R7723 PMT assembly. Only the near periphery is equipped with GD: the fast pulse they produce gets widened by the longer cable thus diminishing the usefulness of the GL. Center temporarily has a second GL with a Hamamatsu H6527 PMT and its calibration is also included in the table.

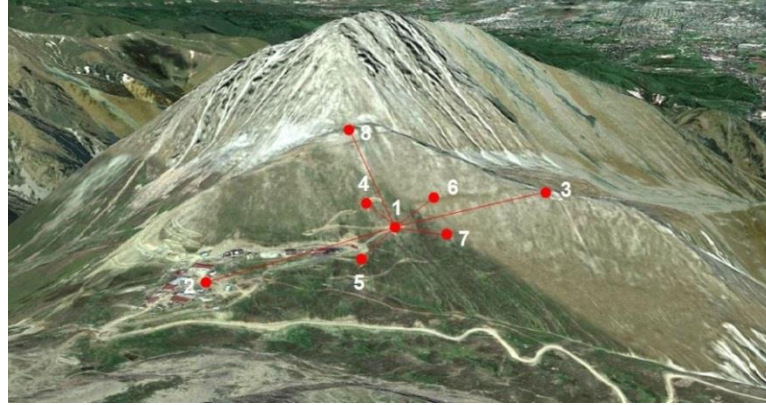


**Figure 1: The bird-eye view of the detector stations positions.**

**Table 1: Coordinates of detection points.**

Station #	X, m	Y, m	Z, m	R, m
1	0	0	0	0
2	-445.9	-85.6	2.8	454.1
3	384.9	79.5	36.1	394.7
4	-55.0	-94.0	31.1	113.3
5	-142.4	36.9	-12.6	147.6
6	151.2	-17.9	31.3	155.4
7	88.6	178.4	-39.0	203.0
8	221.3	262.0	160.7	378.7

The far periphery includes detection points 2, 3 and 8. Far points use only single SD each. They all have PMT-49 (FEU49) by MELZ [9] (replaced with R7723 in March 2017). This is due to the fact that long cables (~500m) are used to connect these points to the Data Acquisition system (DAQ) which is located at detection point 1. The cable calibration [3] shows that signal widening and signal loss become significant in this case, thus justifying the use of FEU49 as they have wider initial pulse. In the upgrade, they were all replaced as outdated.

All SD and GD are pyramid-shaped, the PMT above the center of detection medium at the height of the size of medium size (e.g. 1 m for scintillator and 0.5 m for glass).

For HT, the z-plane is parallel to the sky, the x-axis is directed north. All SD and GL are in the z-plane. There are also x- and y-plane scintillator detectors but they are not currently used. This arrangement is needed for the angular isotropy in the registration of charged particles to be used in the future. Theoretically, better isotropy may be achieved by an upgrade to liquid

scintillators [10] [11] with a symmetric active volume but it is not being yet considered at this time.

### 3. Detectors MIP Response Calibration

Each SD/GD response to MIP is calibrated individually. For that, an additional trigger detector consisting of FEU49 and a 15 cm diameter scintillator is spaced under each detector being calibrated. Double-coincidence schema is used, facilitated by 14bit CAEN [12] DT5730 flash ADC. The setup schematic is shown in Figure 2. The reason for such setup design is that only two cables connect each detection point with DAQ physically.

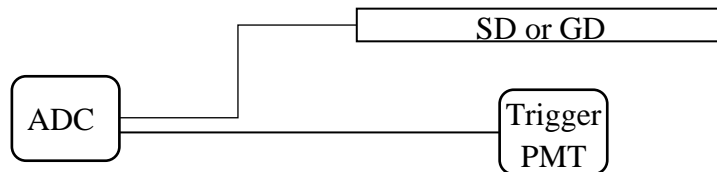


**Figure 2: MIP calibration setup schematic for SD/GD.**

The resulting calibration gives the area of a single MIP signal as well as the width of the MIP signal pulse from each SD. Due to data analysis details, total duration is currently taken as time between the 0.1 and 0.9 of the pulse area; pulse front is defined as time between 0.1 and 0.5 of the pulse area. This reduces the baseline noise effects. The uncertainty, associated with the size of the integration window is included in the total error.

From [1], the pulse front for SD is  $7.16 \pm 0.40$  ns and the total duration is  $21.6 \pm 1.48$  ns with the systematic error of  $\pm 0.10$  ns; the pulse front for GD for one MIP is  $2.17 \pm 0.13$  ns (over 18 m cable) and the total duration is  $5.10 \pm 0.67$  ns with the  $\pm 0.11$  ns systematic error for both.

The normalized area of a MIP signal from a GD from a detection point 1 is shown in Figure 3. The waveform recorded by the ADC consist of 5110 data points digitized every 2 ns each, for the total of  $10.22 \mu\text{s}$ . The full range of  $2^{14}$  bins corresponds to 2 V scale. The areas are given in the custom units of ADC counts  $\cdot$  ns.

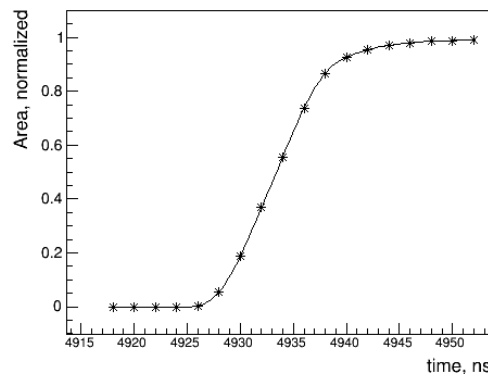


**Figure 3: Normalized integral for MIP pulse from GD.**

As with any calibration, where the detector that is being calibrated is also part of the triggering, there is also a question of the threshold enforced on the detector that is being calibrated. Here we use the threshold as low as possible but still above a pedestal value. For that, a threshold of a few mV is used first and the data is taken with a pedestal clearly visible. Then the data is retaken

with the threshold value right above the pedestal value since for all detectors there is a clear separation between the pedestal and the lowest MIP signal. The Landau curve fit gives the most probable value (MPV) used for the calibration. Care is taken to make sure that chosen threshold value doesn't affect the resulting calibration value (e.g. any possible shift in area MPV is much smaller than the associated uncertainty). The example fit of a MIP signal area for the SD from detection point 1 (Center) is shown in Figure 4. Fit is done using ROOT [13] package PyROOT, areas are found using trapezoidal method [14]. The correspondence of the names of detection points to numbers is given in the Table 2. A fit to a Landau distribution is used since the (relatively) thin target is used.

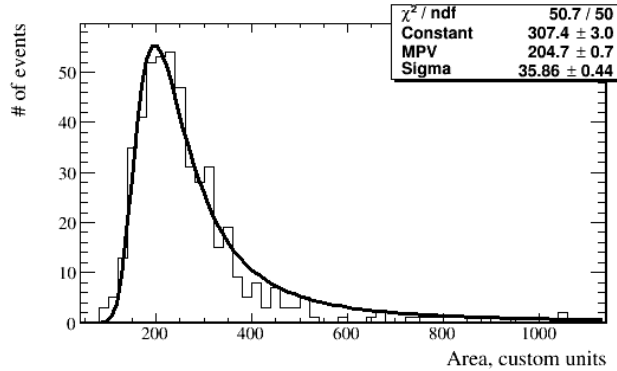


**Figure 4: SD detector response to MIP signal**

**Table 2: Names of detection stations**

<i>Station name</i>	Center	Yastreb ov	Stone Flower	Left	Kurash kin	Right	Bottom	Upper	Cher
<i>Station number</i>	1	2	3	4	5	6	7	8	VCD

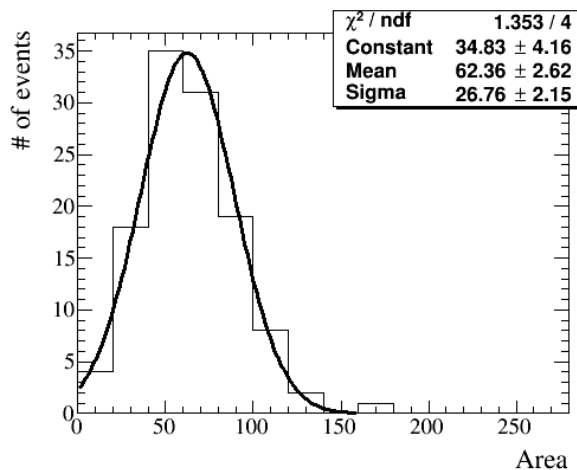


**Figure 5 : R7723 PMT single PE response pulse area at 1700V**

In order to obtain an approximate photon count for each MIP calibration for the match with simulation of the detectors we also do the single photo-electron (PE) R7723 PMT response pulse area calibration. For that, low light LED pulse is fed to PMT connected to DAQ via short cable (<1m). Since signal is baseline subtracted, the pedestal is very low and is removed from later fit. Care is taken to ensure that pedestal has about 80% of all events in order for single photon detection assurance. Figure 5 shows the pulse area of PMT single PE response at 1700V

with pedestal subtracted. PMT is calibrated at the different bias voltages to match different detectors. Signal losses in each cable [3] and presence of impedance matching resistor (if present) must be accounted for when number of photons is accessed for each detector.

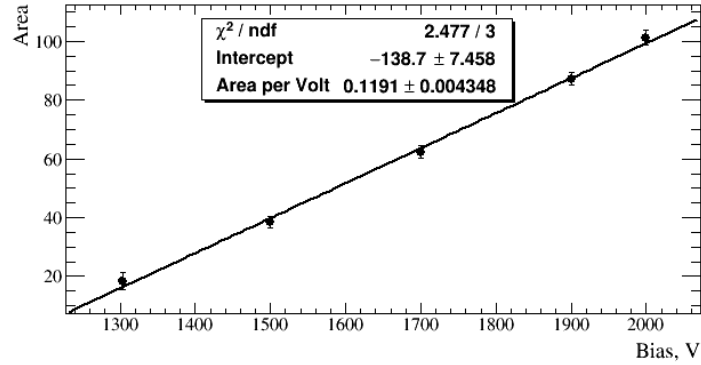


**Figure 6: Single PE pulse area vs. bias voltage for R7723 PMT**

**Table 3: Detector MIP response pulse area at operating bias voltage**

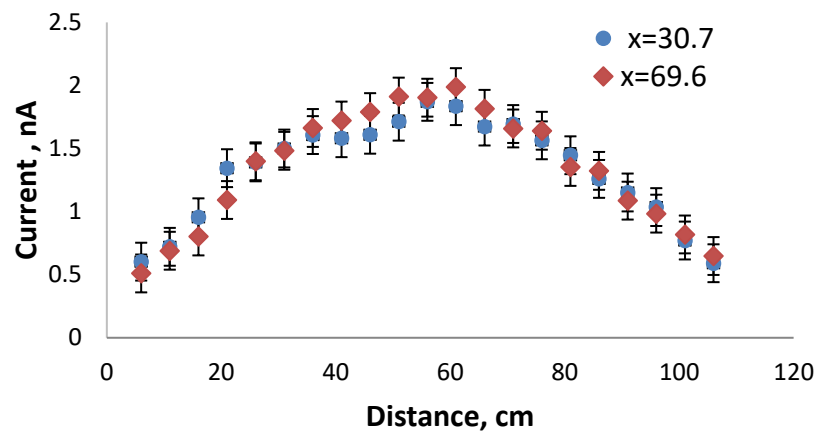
Detection point and cable designation	Detector type	Area (ADC counts · ns)	Detection point and cable designation	Detector type	Area (ADC counts · ns)
Bottom New	SC	529 ± 10 91 ± 7	Left New	SC	574 ± 11 110 ± 8
Bottom Old	GL	134 ± 3 23 ± 2	Left Old	GL	132 ± 2 16 ± 2
Center Blue	Empty		Right New	SC	513 ± 8 78 ± 5
Center Green	Empty		Right Old	GL	137 ± 3 31 ± 2
Center Red (before Oct. 20, 2016)	GL	83 ± 3 22 ± 2	Stone Flower New	SC/FEU49	710 ± 15 201 ± 10
Center Red New	GL	85 ± 3 23 ± 2	Stone Flower Old	Empty	
Center White	Empty		Yastrebov New	SC/FEU49	2110 ± 16 429 ± 11
Center Yellow	SC	470 ± 5 57 ± 6	Yastrebov Old	Empty	
Cher Green Red	Empty		Upper New	SC/FEU49	768 ± 6 124 ± 7
Cher White Blue	VCD		Kurashkin New	SC	549 ± 12 107 ± 8
Cher Yellow	VCD		Kurashkin Old	GL	155 ± 5 50 ± 3
Center Blue New	GL	183 ± 9 44 ± 5	Bottom Old2	Empty	

In Figure 6, the single PE area vs biasing voltage is shown. For the R7723 PMT, we can see that it is linear for a very wide range of biases, with 2000V being recommended maximum and pulses becoming too close to noise floor below 1300V for accurate calibration.

The results of the MIP calibration are in Table 3. Only values at used operating biases are shown per detector per cable. The full calibration table is in Appendix I. All cable effects are included in the calibration; MPV (top value) and  $\sigma$  (bottom value) with corresponding fit uncertainties are listed.

#### 4. SD Detector Response Uniformity

For SD detectors, due to the PMT placement above the scintillator center within pyramid-shaped enclosure, the non-uniformity of particle detection from scintillator center and edges exists. In order to accurately assess the charged particles flux through each SD, this non-uniformity should be measured.



For this purpose, each SD is scanned using  $^{60}\text{Co}$  radioactive source across the scintillator side along four lines: both diagonals and two lines, passing through centers of parallel sides in x and in y in scintillator plane. From the data, an average weight of  $0.70 \pm 0.06$  is calculated that is later applied to MIP calibration for each SD detector. The GD uniformity is  $0.74 \pm 0.04$  [7].

#### 5. Cherenkov Detector

The Vavilov-Cherenkov Detector (VCD) is located next to detection point 1 as close to DAQ system as possible. The VCD consists of three parabolic mirrors of 150cm diameter with 65cm focal length each mounted on the rotating support allowing registration of radiation in zenith angle range of  $0^\circ$ - $80^\circ$  and azimuthal angle range of  $0^\circ$ - $360^\circ$ . There is a PMT-49 (FEU49B) and a Hamamatsu H6527 PMT located in the focal point of two lower mirrors. Both are 15cm cathode diameter PMTs with the spectral response from 360 nm to 600 nm. The angle of view for each mirror is  $\sim 13^\circ$ . For completeness, we mention the VCD but its calibration is not included here. Note that PMTs are very easily damaged by the light, thus a future upgrade may include the Geiger-mode avalanche photodetector [15] [16] arrays [17] since they are unaffected by high light intensity such as moonlight or car headlights. These are fast detectors and have been used on a large scale [18]. Both VCD channels are connected to DAQ using separate cable each.

## 6. Conclusion

The MIP calibration of the HT detector system was carried out for both SD and GL detectors at different biasing voltages. The uniformity of response for these detectors was measured as well. A detector upgrade is planned so this note will not be updated and will be valid for data before March 2017

## Bibliography

- [1] RU Beisembaev, EA Beisembaeva, OD Dalkarov, VA Ryabov, AV Stepanov, NG Vildanov, MI Vildanova, VV Zhukov, KA Baigarin, D Beznosko, TX Sadykov, NS Suleymenov, "The 'Horizon-T' Experiment: Extensive Air Showers Detection," *arXiv:1605.05179 [physics.ins-det]*, May 17 2016.
- [2] D. Beznosko et al., "Horizon-T Extensive Air Showers detector system operations and performance," in *PoS(ICHEP2016)784, proceedings of ICHep2016*, Chicago, 2016.
- [3] D Beznosko, T Beremkulov, A Iakovlev, Z Makhataeva, M I Vildanova, K Yelshibekov, V V Zhukov, "Horizon-T Experiment Calibrations-Cables," *arXiv:1608.04312*, 8/2016.
- [4] Duspayev et al., "The distributed particle detectors and data acquisition modules for Extensive Air Shower measurements at "Horizon-T KZ" experiment," in *PoS(PhotoDet2015)056, in proceedings to PhotoDet2015 conference*, Moscow, 2015.
- [5] A. Dyshkant, D. Beznosko, G. Blazey, E. Fisk, E. Hahn, V. Rykalin, M. Wayne and V. Zutshi, "SCINTILLATION DETECTORS-Quality Control Studies of Wavelength Shifting Fibers for a Scintillator-Based Tail Catcher Muon Tracker for Linear Collider Prototype Detector," *IEEE Transactions on Nuclear Science*, volume 53, issue 6, page 3944, 2006.
- [6] Adil Baitenov, Alexander Iakovlev, Dmitriy Beznosko, "Technical manual: a survey of scintillating medium for high-energy particle detection," *arXiv:1601.00086*, 2016/1/1.
- [7] M. Yessenov, A. Duspayev, T. Beremkulov, D. Beznosko, A. Iakovlev, M.I. Vildanova, K. Yelshibekov, V.V. Zhukov, "Glass-based charged particle detector performance for Horizon-T EAS detector system," *arxiv:1703.07919*, 03/2017.
- [8] Hamamatsu Corporation, 360 Foothill Road, PO Box 6910, Bridgewater, NJ 08807-0919, USA; 314-5, Shimokanzo, Toyooka-village, Iwatagun, Shizuoka-ken, 438-0193 Japan.
- [9] MELZ-FEU, 4922-y pr-d, 4c5, Zelenograd, g. Moskva, Russia, 124482 (<http://www.melz-feu.ru>).
- [10] L. J. Bignell et al., "Characterization and Modeling of a Water-based Liquid Scintillator," *Journal of Instrumentation*, IOP Publishing, vol. 10, p. 12009, 12/2015.
- [11] D. Beznosko, "Performance of Water-based Liquid Scintillator," *American Physical Society, APS*, April Meeting 2013, April 13-16, 2013.
- [12] CAEN S.p.A. Via della Vetraria, 11, 55049 Viareggio Lucca, Italy. <http://caen.it>.

- [13] R. Brun, F. Rademakers, "ROOT: An object oriented data analysis framework," *Nucl. Instrum. Meth. A*, vol. 389, p. 81–86, 1997.
- [14] "numpy.trapz," [Online]. Available: <http://docs.scipy.org/doc/numpy-1.10.1/reference/generated/numpy.trapz.html>.
- [15] D. Beznosko, "Novel multi-pixel silicon photon detectors and applications in T2K," *arXiv:0910.4429*, 2009.
- [16] T Beremkulov et al., "Random Number Hardware Generator Using Geiger-Mode Avalanche Photo Detector," *arXiv:1501.05521*, Jan 2015.
- [17] D. Beznosko, A. Dyshkant, C.K. Jung, C. McGrew, A. Pla-Dalmau, V. Rykalin, "MRS Photodiode Coupling with Extruded Scintillator via Y7 and Y11 WLS Fibers," February FERMILAB-FN-0796, 2007.
- [18] S Assylbekov et al., "The T2K ND280 off-axis pi-zero detector," *Nuclear Instruments and Methods in Physics Research Section A*, vol. 686, pp. 48-63, 2012/9/11.
- [19] D. Beznosko, G. Blazey, A. Dyshkant, V. Rykalin, J. Schellpffer and V. Zutshi, "Modular Design for Narrow Scintillating Cells with MRS Photodiodes in Strong Magnetic Field for ILC Detector," *Nuclear Instruments and Methods in Physics Research Section A*, Volume 564, pages 178-184, 2006/8/1.
- [20] K. Abe et al., "The T2K Experiment," *NIM A* Jun 06, 2011 NIMA-D-11-00462R1, doi: 10.1016/j.nima.2011.06.067, arXiv:1106.1238 [physics.ins-det].
- [21] D. Beznosko, G. Blazey, A. Dyshkant, V. Rykalin, V. Zutshi, "Effects of the Strong Magnetic Field on LED, Extruded Scintillator and MRS Photodiode," *NIM A*, vol. 553, pp. 438-447, 2005.
- [22] D. Beznosko, T. Beremkulov, A. Duspayev, A. Iakovlev, "Random Number Hardware Generator Using Geiger-Mode Avalanche Photo Detector," in *PoS(PhotoDet2015)049*, in *proceedings to PhotoDet2015*, Moscow, 2015.



## Appendix I

Calibrations valid before March 2017. Updated version will be uploaded as a separate document as some detectors were changed in HT

MIP calibration for all scintillator detectors at different bias voltages. In green is the current operation bias.

Name	Voltage	MPV	MPV Error	sigma	Sigma Error
Bottom SC	1100	218.4	4.5	44.2	2.5
	1200	342.7	7.3	60.8	3.7
	1250	418.1	8	76.5	4.9
	1300	528.6	10	90.9	6.6
	1350	629.7	13.8	109.8	8.7
	1400	694.3	13.4	123.2	8.3
Kurashkin SC	1200	412.2	7.1	68.9	4.6
	1250	462.1	7.5	80.8	5.1
	1300	549.1	12.3	106.9	7.6
	1400	765.1	14.6	138.4	11.2
Left SC	1100	370.7	2.8	61.4	1.6
	1200	488.1	7.5	81.9	4.7
	1250	573.8	11	109.8	7.7
	1300	678.7	14	125.3	8.8
	1400	929.7	23	212.4	16.1
Right SC	1200	396.5	5.1	50.9	2.7
	1300	512.7	7.9	78.3	4.6
	1350	602.1	9.2	93.2	5.7
	1400	687.4	10.2	110.5	6.1
	1500	900.5	15.3	160.8	9.8
St Flower SC	1862	710	15	201	10
Upper SC	1700	768	6	124	7
Yastrebov SC	1800	615	10	221	4
	1900	695	12	253	5
	2000	1050	12	300	9
	2100	1420	25	370	13
	2200	2110	16	429	11
	2300	2695	15	536	11
Center SC	1000	200	4	37.3	0.5
	1100	260	5	35.2	2.2
	1200	470	5	56.8	6
	1500	1160	6	205	6
Bottom Gl	1600	57.9	2.4	22.9	1.5
	1700	70.5	2	20.2	1.2
	1800	91.3	2.1	22.2	1.2
	1900	113	2.2	23.1	1.5
	2000	134	2.6	23.2	1.5
	2100	148	3	27.9	1.9
Left Gl	1700	99.7	2.5	17.7	1.8
	1800	115	2.4	19.9	1.8
	1900	132	2.1	16	1.6

	2000	157.5	3.3	26.3	2.24
Right GI	1800	64.2	2.3	20.9	1.6
	1900	95.1	2.8	27.3	1.8
	2000	136.7	3.2	30.9	2
	2100	173.4	3.5	34.2	2.2
Center GI Big	1400	137.1	2.2	26.9	1.3
	1500	182.6	8.5	43.6	5.2
	1600	247.5	5.6	43.1	3.9
	1700	422	9	79	6
Kurashkin GI	1800	91.2	3.6	22.9	2.2
	1900	155.4	4.8	50.2	2.9
	2000	214.9	6.7	60.3	3.5
	2100	274.1	23.6	75.8	8.4
Center GI 2cm	1700	61.7	2.2	20.1	1.1
	1800	68.9	2	18.9	1.2
	1900	76.4	1.7	15.6	1.2
	2000	84.5	2.4	22.7	1.4
Center GI 3cm	1900	83.1	2.4	22.1	1.4